Gauge effects in bound-bound Rydberg transition matrix elements

A. Duspayev [*] and G. Raithel

Department of Physics, University of Michigan, Ann Arbor, Michigan 48109, USA

Accurate data on electric-dipole transition matrix elements (EDTMs) for bound-bound Rydberg-atom transitions have become increasingly important in science and technology. Here we compute radial EDTMs of rubidium in length, velocity, and acceleration forms for electric-dipole-allowed transitions between states with principal and angular-momentum quantum numbers n and ℓ ranging from 15 to 100. Wave functions are computed based upon model potentials from [Phys. Rev. A **49**, 982 (1994)]. Length-gauge EDTMs of strong low-ℓ Rydberg transitions, often employed in research and technology, are found to deviate from the fundamentally more accurate velocity-gauge form by approximately-n-independent and series-dependent shifts. The shift amount peaks at about 0.34 ea_0 for the Rb $nD \leftrightarrow (n+1)P$ series, a particularly strong Rydberg-transition series in Rb. The shift corresponds to relative EDTM corrections of up to $\approx 10^{-3}$, which can be of concern in high-precision applications. We discuss the physical reasons for the observed gauge differences, explain the conditions for applicability of the velocity- and length-gauge forms for different transition series, and present a decision tree of how to choose EDTMs.

I. INTRODUCTION

Rydberg atoms [1] are an active field of modern physics with applications in precision measurements [2–5], molecular physics [6,7], quantum control [8,9], field sensing [10–13], nonlinear quantum optics [14–16], and as a platform for quantum computing and simulations [17–19]. Being at the core of several directions in fundamental research and emerging quantum technologies [20], Rydberg transitions from low-lying states or other Rydberg atomic states require accurate calculations [21,22]. Of particular interest are electric and magnetic multipole transition matrix elements [23], static and dynamic polarizabilities [21,24], and collisional and photoionization [25–28] cross sections. Among the former, electric-dipole transition matrix elements (EDTMs) are the most important due to their wide usage [21].

A common framework for the computation of EDTMs between different bound Rydberg levels is based on model potentials [29]. In most cases, the computations are performed in the length gauge (LG) [30,31], also referred to as Babushkin gauge [32]. Another common form is the velocity gauge (VG). In addition, there exists an acceleration gauge (AG). Although quantum mechanics is gauge invariant [30,33,34], different approximations and assumptions must be made to transform the expressions for EDTMs between different gauges, which can result in notable discrepancies in the final results [35,36]. These are revealed in high-precision calculations and naturally raise the question which gauge should be used. This issue has been discussed in a range of research fields, including interaction of atoms and molecules with strong fields [37–42], solid-state physics [43,44], and astrophysical spectroscopy [32,45].

Gauge invariance of atomic polarizability has been shown in Ref. [34]. To our knowledge, gauge effects in EDTMs have not been broadly discussed yet in context with emerging applications of resonant Rydberg-atom transitions in the aforementioned quantum technologies. Here we provide a comparison of EDTMs computed in the LG, VG, and AG gauges for electric-dipole electromagnetic transitions in rubidium Rydberg atoms. The emphasis is on the LG and VG forms, the most widely used and the most accurate gauges, respectively, while the less accurate AG is discussed for
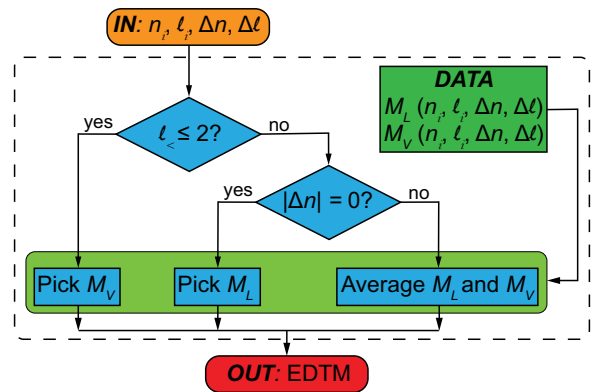

FIG. 1. Decision tree to select EDTMs from precomputed length-gauge and velocity-gauge databases of EDTMs, $M_L(n_i, \ell_i, \Delta n, \Delta \ell)$ and $M_V(n_i, \ell_i, \Delta n, \Delta \ell)$, respectively. Initial- and final-state principal and angular-momentum quantum numbers are denoted (n_i, ℓ_i) and (n_f, ℓ_f), respectively, the difference $\Delta n = n_f - n_i$, the difference $\Delta \ell = \ell_f - \ell_i = \pm 1$, and $\ell_<$ is the lesser of ℓ_i and ℓ_f.

_____
*alisherd@umich.edu

instructive purposes. We show that the angular-momentum type of the Rydberg-Rydberg transition plays a decisive role in what is the best choice for the gauge that should be used. For the Rb model potentials [29] that we use to compute the Rydberg-electron wave functions, we find that the VG should be used if the lesser of the involved angular momenta, $\ell_<$, is two or lower, and that the VG or the LG can be used otherwise, as they produce identical results within the numerical accuracy level of the calculations. As an exception, only the LG should be used for transitions between near-degenerate Rydberg levels with $l_< \geqslant 3$. The decision tree that follows is summarized in Fig. 1 and is rationalized throughout the paper.

The paper is organized as follows: The three gauge forms are reviewed and the relevant expressions are provided in Sec. II, the results are presented in Sec. III and discussed in Sec. IV. The paper in concluded in Sec. V.

II. MATRIX ELEMENTS IN DIFFERENT GAUGE FORMS

In this section, we review the formalism for calculations of EDTMs in the three gauges, and justify the validity of the electric-dipole approximation (EDA). We begin with a spin-less, nonrelativistic N-electron atom with nuclear charge Z placed in a plane-wave electromagnetic field. In the velocity gauge, the linearly polarized field has a vector potential $\mathbf{A}(\mathbf{r}, t) = \mathbf{A}_0 \sin(\mathbf{k} \cdot \mathbf{r} - \omega t)$, wave vector $\mathbf{k}$, angular frequency ω, and an amplitude of the electric field of $E_0 = \omega A_0$. The atom can be described by the following Hamiltonian:

$$\hat{H} = \hat{H}_0 + \hat{H}_{\text{int}}, \qquad (1)$$

where the field-free part, $\hat{H}_0$, is (in SI units)

$$\hat{H}_0 = \sum_{i=1}^{N} \left(\frac{\hat{\mathbf{p}}_i^2}{2m_e} - \frac{Ze^2}{4\pi\epsilon_0 \hat{r}_i} \right) + \frac{1}{4\pi\epsilon_0} \sum_{\substack{i=1 \\ i \neq j}}^{N} \frac{e^2}{|\hat{\mathbf{r}}_i - \hat{\mathbf{r}}_j|}, \quad (2)$$

and the atom-field interaction part, $\hat{H}_{\text{int}}$, resulting from including the kinetic momentum, $\hat{\mathbf{P}}_i = \hat{\mathbf{p}}_i + e\hat{\mathbf{A}}(\hat{\mathbf{r}}_i, t)$, is

$$\hat{H}_{\text{int}} = \sum_{i=1}^{N} \left(\frac{e}{2m_e} [\hat{\mathbf{p}}_i \cdot \mathbf{A}(\hat{\mathbf{r}}_i, t) + \mathbf{A}(\hat{\mathbf{r}}_i, t) \cdot \hat{\mathbf{p}}_i] + \frac{e^2 \mathbf{A}^2(\hat{\mathbf{r}}_i, t)}{2m_e} \right). \qquad (3)$$

Here, e is the magnitude of the electron charge, m_e is the electron mass, and $\hat{\mathbf{r}}_i$ are the position operators of the electrons. The $\mathbf{A}^2$ term in Eq. (3) describes the ponderomotive interaction, which can be employed to realize ponderomotive optical lattices for Rydberg atoms [46,47]. In the present work, we focus on the first term, which describes, among other phenomena, Rydberg-atom microwave transitions.

We consider an alkali-metal atom with a single electron excited into a Rydberg state. The sum in Eq. (3) can be dropped, and the interactions of the Rydberg electron with the core electrons can be compounded into a set of ℓ-specific model potentials [29]. The vector potential specified above satisfies the Coulomb-gauge condition, $\nabla \cdot \mathbf{A} = 0$, in which $\hat{\mathbf{p}}$ and $\mathbf{A}(\hat{\mathbf{r}}_i)$ commute. Dropping the $\mathbf{A}^2$ term, which is irrelevant for the low-field transitions considered here, Eq. (3) can be written as

$$\hat{H}_{\text{int}} = \frac{e}{m_e} \mathbf{A}(\hat{\mathbf{r}}) \cdot \hat{\mathbf{p}}. \qquad (4)$$

We then express the electric-field-normalized atom-field interaction matrix element between initial $|i\rangle$ and final $|f\rangle$ states of the Rydberg atom, in the rotating-wave approximation, as

$$M_V = \frac{\langle f | \hat{H}_{\text{int}} | i \rangle}{(E_0/2)} = -\frac{e\hbar}{m_e\omega} \left(\hat{\mathbf{n}} \cdot \int \psi_f^* e^{i\mathbf{k}\cdot\mathbf{r}} \nabla \psi_i d^3r \right).$$

Making the electric-dipole approximation (EDA), which is valid for microwave transitions of Rydberg atoms, as discussed below,

$$M_V = -\frac{e\hbar}{m_e\omega} \left(\hat{\mathbf{n}} \cdot \int \psi_f^* \nabla \psi_i d^3r \right), \qquad (5)$$

where $\hat{\mathbf{n}}$ is the electric field's polarization vector. The electric-dipole transition matrix element (EDTM) in Eq. (5) is commonly referred to as the velocity (VG) form, because it involves the linear-momentum operator. To transform it into the often-used length-gauge (LG) form, one invokes the commutation relation $[\hat{\mathbf{r}}, \hat{H}_0] = \frac{i\hbar}{m_e}\hat{\mathbf{p}}$, which is exact only if $\hat{H}_0$ does not contain momentum-dependent potentials [30]. For the case of an on-resonant interaction, $\omega = |E_f - E_i|/\hbar$, with final- and initial-state energies E_f and E_i, respectively, the frequency denominator in Eq. (5) drops out, and the EDTM takes the most commonly employed LG form,

$$M_L = e \left(\hat{\mathbf{n}} \cdot \int \psi_f^* \mathbf{r} \psi_i d^3r \right). \qquad (6)$$

For the acceleration-gauge (AG) form to be valid, the valence-electron potential in $\hat{H}_0$ must be of pure Coulomb form, $\hat{V} = -e^2/(4\pi\epsilon_0 \hat{r})$, such that the commutation relation $[\hat{\mathbf{p}}, \hat{H}_0] = -i\hbar\nabla\hat{V}$ is true [30]. Then, the EDTM for a resonant interaction can be expressed in AG form,

$$M_A = \frac{e^3}{4\pi\epsilon_0 m_e\omega^2} \left(\hat{\mathbf{n}} \cdot \int \psi_f^* \frac{\hat{\mathbf{r}}}{r^3} \psi_i d^3r \right). \qquad (7)$$

The EDTMs obtained from Eqs. (5)–(7) are in SI units; in the next section we convert them into atomic units by dividing by ea_0, where a_0 is the Bohr radius. To convert Eqs. (5)–(7) themselves, set $\hbar = m_e = e = 4\pi\epsilon_0 = 1$.

The VG form is the most generally applicable, original form, whereas for the LG and AG forms to be applicable specific requirements must be satisfied. These hold in the nonrelativistic hydrogen atom. However, the alkali model potentials [29], which we use here, are ℓ dependent for $\ell \leqslant 3$ and the same for $\ell \geqslant 3$, which makes the LG form inaccurate if $\ell_< \leqslant 2$ (where $\ell_<$ is the lesser of ℓ_i and ℓ_f). In the main part of our work, we quantify the deviations of EDTMs computed in the LG form from those in the fundamentally accurate VG form.

Rydberg atoms with a polarizable ionic core, such as Rb and Cs, also exhibit a long-range, non-Coulombic core-polarization potential the leading term of which scales as $-\alpha_d/(2r^4)$. There, α_d is the dipolar core polarizability. The polarization potential applies to all ℓ values, making the AG form inaccurate for all ℓ.

It is noteworthy that the EDA must be applied to the VG form of the EDTM, which follows directly from the $\mathbf{A} \cdot \mathbf{p}$ part of the minimal-coupling Hamiltonian in Eq. (4), before the matrix element can be transformed into the LG and AG

forms (under the applicable respective conditions). For the microwave transitions considered in the present work, the EDA is naturally satisfied due to the long radiation wavelength ($\mathbf{k} \cdot \mathbf{r} \ll 1$). It has been shown elsewhere that the EDA even applies in the UV wavelength range [28], where the Rydberg-atom size typically exceeds the wavelength ($\mathbf{k} \cdot \mathbf{r} > 1$).

In the numerical results in Sec. III, we show comparisons between the EDTMs for a representative selection of transition series. All EDTMs shown are radial parts; matrix elements for transitions with specific magnetic quantum numbers follow from multiplication with angular matrix elements provided, for instance, in Ref. [30].

The fine structure of the Rydberg levels is ignored in our analysis, because it would primarily only add Clebsch-Gordon factors to the angular matrix elements. The gauge effects we focus on in our work result from the ℓ dependent and non-Coulombic long-range terms in the model potentials [29] used to compute the radial wave functions of the (n, ℓ) states of the atom. To capture gauge effects, it is therefore sufficient to consider radial EDTMs with fine-structure-averaged quantum defects [1] for the Rydberg energy levels.

For the numerical calculation of the required wave functions, we use a method described in Ref. [48] that allows a nonuniform spatial grid. The spatial finesse is characterized by a specifiable number of grid points per local de Broglie wavelength of the electron wave-function (which varies widely within the atomic potential). For the bulk of our calculations, we chose a lower limit of 5000 grid points per electron wavelength. To estimate numerical uncertainty, several computation series were performed on finer grids with a minimum of 10 000 grid points per electron wavelength. All computations were performed in Fortran using REAL*16 precision. For reference, less than 500 grid points per electron wavelength, in a REAL*8 implementation, suffice to compute EDTMs of strong bound-bound Rydberg transitions with three to four significant digits.

III. RESULTS

We have computed the EDTMs in all three gauge forms for all electric-dipole-allowed Rydberg-Rydberg transitions $n_i \rightarrow n_f$, with initial n_i and final n_f principal quantum numbers covering the full range from 15 to 100, and for all combinations of initial and final angular momenta, ℓ_i and ℓ_f, that satisfy the electric-dipole selection rule $\Delta\ell = \ell_f - \ell_i = \pm 1$. The results are stored in data banks $M_V(n_i, \ell_i, \Delta n, \Delta\ell)$, $M_L(n_i, \ell_i, \Delta n, \Delta\ell)$, and $M_A(n_i, \ell_i, \Delta n, \Delta\ell)$, with Δn defined as $\Delta n = n_f - n_i$. The computed data for the transitions used in Fig. 2 is presented in the Supplemental Material [49].

As convenient measures for the radial EDTMs and for the differences between them in the three gauge forms, we define the scaled dipole moments, the absolute gauge error, and the relative gauge error as

$$\tilde{M}_j = \frac{M_j}{n_i^* n_f^*}, \qquad j = V, L, A,$$

$$\Delta_{j,V} = M_j - M_V, \quad j = L, A, \qquad (8)$$

$$\delta_{j,V} = \left| \frac{\Delta_{j,V}}{M_V} \right|, \qquad j = L, A,$$

where the subscripts V, L, and A stand for VG, LG, and AG forms of the EDTMs, respectively. The effective quantum numbers are $n_i^* = n_i - \delta_{\ell_i}$ and $n_f^* = n_f - \delta_{\ell_f}$, with quantum defects δ_{ℓ_i} and δ_{ℓ_f} [1].

In Fig. 2, we show $|\tilde{M}_V|$, $\Delta_{L,V}$ and $\delta_{L,V}$ vs n_i for several transition series with $\ell_< \leqslant 2$. We consider transitions with $|\Delta n| \leqslant 4$, which include the series with the largest EDTMs. These series are used in most applications.

Rb $n_iS_{1/2} \leftrightarrow n_fP_J$ microwave transitions are of some importance because $n_iS_{1/2}$ Rydberg atoms can be initialized by two-photon laser excitation from the Rb $5S_{1/2}$ ground state. The EDTMs for the various series in this type scale as $n_i^* n_f^*$, as the scaled values in Fig. 2(a) are approximately n independent within each series. This behavior is fairly typical (but not guaranteed) for Rydberg transitions, because it essentially means that the EDTMs scale with the atomic radius, which is $\approx 2n^2$ for low-ℓ states [1]. Interestingly, as seen in Fig. 2(b), the absolute gauge errors $\Delta_{L,V}$ take series-dependent values with no significant n dependence. For the strongest series, $nS \leftrightarrow nP$ and $nS \leftrightarrow (n-1)P$, it is $\Delta_{L,V} \approx -0.062\ ea_0$ and $-0.058\ ea_0$, respectively. For the weaker series, the values of $\Delta_{L,V}$ generally drop. For instance, for the $nS \leftrightarrow (n+4)P$ series it is $\Delta_{L,V} \approx -0.0066\ ea_0$. The constancy of the $\Delta_{L,V}$ is explained in Sec. IV. The relative gauge error, $\delta_{L,V}$, typically ranges between 10^{-4} and 10^{-5} for the strongest transitions, $nS \leftrightarrow nP$ and $nS \leftrightarrow (n-1)P$, as seen in Fig. 2(c), while for the weaker transitions with larger $|\Delta n|$ this number can be as large as $\approx 10^{-3}$.

Rb $n_iD \leftrightarrow n_fP$ microwave transitions are often used because of the large values of $|M_V|$ on the nD to $(n+1)P$ series, and because the two-photon laser preparation rates of n_iD Rydberg atoms from the Rb $5S_{1/2}$ ground state are greater than those of n_iS Rydberg atoms. Fig. 2(d) shows that the EDTMs of the strong $n_iD \leftrightarrow (n_i + \Delta n)P$, $\Delta n \geqslant 1$, series scale as n^2. However, the weak series, which have $\Delta n \leqslant 0$, do not scale. The EDTMs of the $nD \leftrightarrow nP$ series even pass through a pronounced minimum of $|M_V| \approx 0.16\ ea_0$ at $n = 20$, which is about three orders of magnitude lower than the $|M_V|$ value of the nearby $20D \leftrightarrow 21P$ transition (which has $|M_V| = 472\ ea_0$). The unusual behavior of the $nD \leftrightarrow nP$ series can be attributed to the exact level energies and wave functions of the involved states, which depend on the Rb quantum defects of both initial and final levels. The EDTM minimum at $n = 20$ may thus be characterized as a bound-bound analog of a Cooper minimum [27,50]. A Cooper minimum [50] is a type of minimum of the photoionization cross-section versus light wavelength. Due to the resemblance in the physical origins of Cooper minima and the EDTM minimum at $n = 20$ and analogous instances identified below, we will refer to such minima as "Cooper-like minima." The absolute gauge errors $\Delta_{L,V}$ again have approximately n-independent but series-dependent values. The strongest of all series in Fig. 2, the $nD \leftrightarrow (n+1)P$ series, has $\Delta_{L,V} \approx -0.34\ ea_0$ [see Fig. 2(e)]. The relative gauge errors, $\delta_{L,V}$, are on the order of three times larger than those of comparable $n_iS \leftrightarrow n_fP$ transitions, with numerous instances of $\delta_{L,V} > 10^{-2}$ [see Fig. 2(f)]. The relative gauge error reaches a high of ≈ 0.5 for the $20D \leftrightarrow 20P$ Cooper-like minimum.

In Figs. 2(g)–2(i) we show data on several $n_iD \leftrightarrow n_fF$ series. Figures 2(d) and 2(g) have some resemblance, which
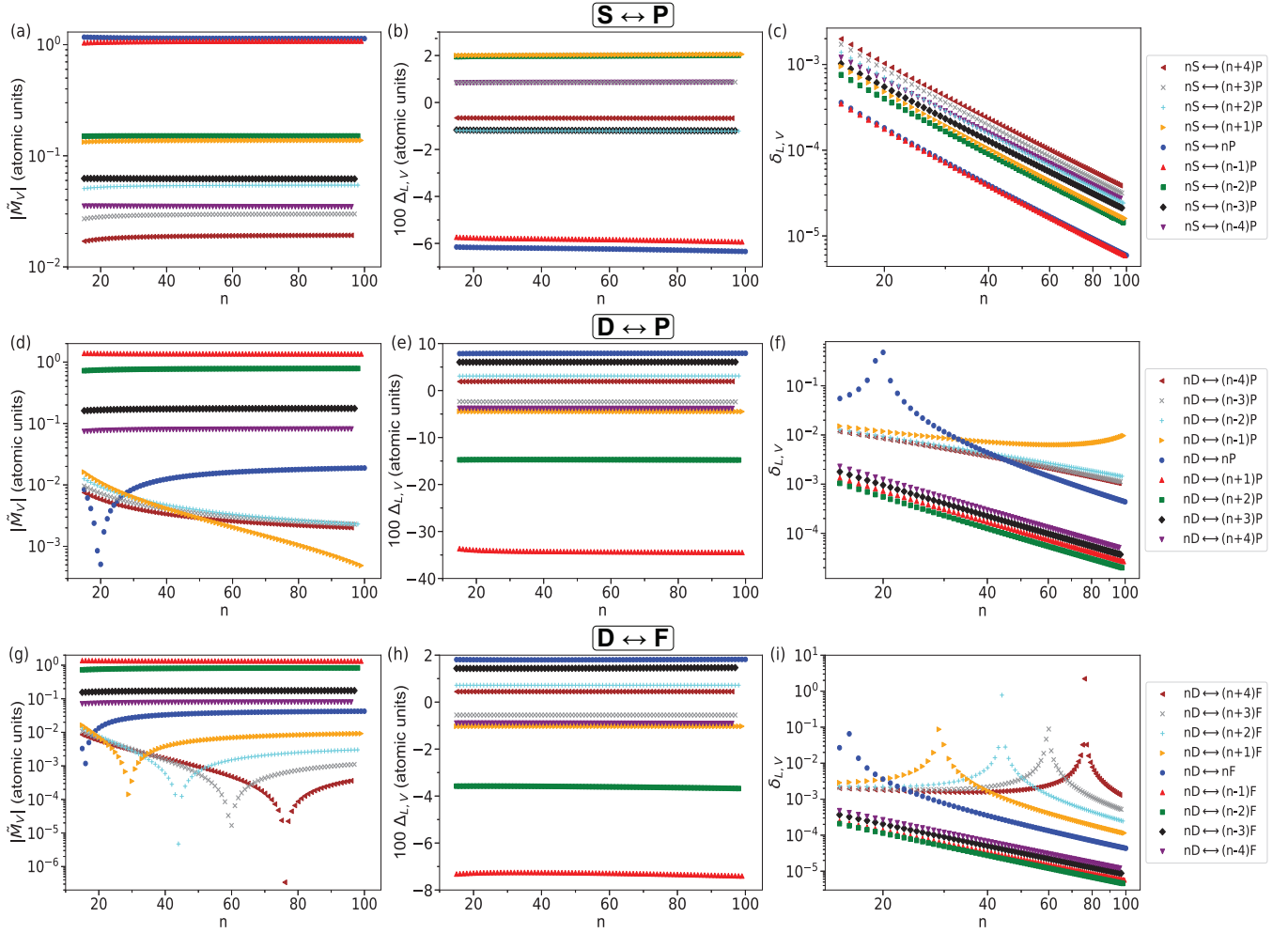
FIG. 2. The columns show, from left to right, the scaled EDTMs in VG form, $\tilde{M}_V$, the absolute gauge errors, $\Delta_{L,V}$, and the relative gauge errors, $\delta_{L,V}$, as a function of $n = n_i$. Note the $100\times$ enlargement on the $\Delta_{L,V}$ scales. The first row, panels (a)–(c), is for the indicated $n_iS \leftrightarrow n_fP$ series, the second row, panels (d)–(f), is for a set of $n_iD \leftrightarrow n_fP$ series, and the last row, panels (g)–(i), is for a set of $n_iD \leftrightarrow n_fF$ series. The data used for this figure is listed in the Supplemental Material [49].

one may attribute to similar differences in the quantum defects of the respective involved states. For the $n_iD \leftrightarrow (n_i + \Delta n)F$ series, the EDTMs of the $\Delta n \leqslant -1$ cases are large and scale with n^2, while the $\Delta n \geqslant 0$ cases have small EDTMs and show Cooper-like minima, similar to the $nD \leftrightarrow nP$ series in Fig. 2(d). Since the $\Delta_{L,V}$ values are approximately n independent and series specific [see Fig. 2(h)], the relative gauge errors $\delta_{L,V}$ again reach values near 1 at the Cooper-like minima [see Fig. 2(i)].

For $\ell \geqslant 3$, the utilized model potentials become ℓ independent, and numerical readings of $\Delta_{L,V} \neq 0$ are only due to numerical errors. In our work, the relative numerical confidence level of the EDTMs is $\approx 10^{-5}$ or better. The numerical uncertainty was verified by comparing several results from Fig. 2 with similar results obtained with a finer spatial grid in the wave-function calculations, and by verifying that the conjugate of Eq. (5) yields the same results as Eq. (5), within the numerical error. The estimation of the numerical error is important because it proves that the deviations between M_L and M_V shown in Fig. 2 are indeed due to the different gauge forms used

in the EDTM calculations. Further proof is given in the Discussion.

Finally, we show a comparison between EDTMs computed in AG and VG forms. This comparison is of instructional interest, but it is not relevant to applications of EDTMs because the AG is fundamentally invalid for all ℓ. For low-ℓ transitions, $\delta_{A,V}$ can reach very large values (up to $\approx 10^6$, not shown here), reflecting the invalidity of the AG form for non-Coulombic potentials. However, if ℓ becomes sufficiently large, the EDTMs in AG form tend to gradually approach the correct EDTMs obtained from the other forms. As an example, in Fig. 3 we show results for several series for transitions between $\ell_i = 10$ and $\ell_f = 11$ states. On the series shown, the error of the AG form is small but exceeds the numerical error by several orders of magnitude. While $\Delta_{A,V}$ does not exhibit a simple scaling in n_i, its rapid rise in magnitude with n_i stands in contrast with Figs. 2(b), 2(e), and 2(h). In additional analyses, not presented, we have found that $\Delta_{A,V}$ drops below our numerical error for $\ell \gtrsim 20$. Hence, within our numerical error, the non-Coulombic polarization potential, $-\alpha_d/(2r^4)$, becomes inconsequential to the EDTMs
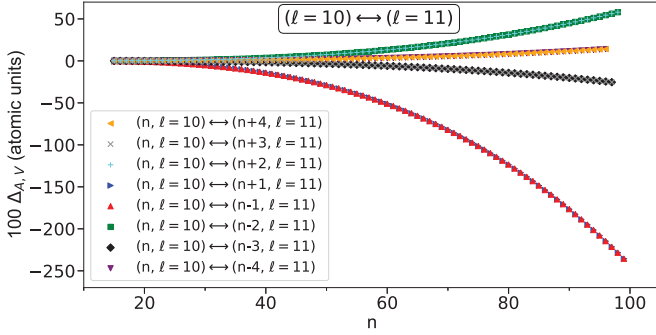
FIG. 3. Absolute gauge error of the AG vs the VG form, $\Delta_{A,V}$, versus $n = n_i$ for the indicated transition series with $\ell_{i/f} = 10$ or 11. Note the $100\times$ enlargement on the $\Delta_{A,V}$ scale.

for $\ell \gtrsim 20$. Then, the net potential takes a practically pure Coulomb form, and the AG results become accurate. Nonetheless, the AG form should not be used because the conditions for its applicability are generally not satisfied in alkali-metal atoms.

IV. DISCUSSION

In Sec. III we have established and quantified deviations between LG and VG computations of EDTMs for transitions that involve Rydberg levels with $\ell_< \leqslant 2$. These deviations are caused by the dependence of the model potentials [29] utilized on ℓ for $\ell \leqslant 3$. For transitions with $\ell_< \geqslant 3$, the model potentials are identical, and the EDTMs in LG and VG forms agree within our numerical error of $\delta_{L,V}$ of $<10^{-5}$.

An intriguing finding in Fig. 2 is that, within any given series, the absolute gauge error $\Delta_{L,V}$ is approximately n independent, regardless of any added complexities such as Cooper-minimum-like behavior in $|M_V|$. In the following we show that this is expected. We find by evaluating matrix elements of the operator difference $[\hat{H}_0, \hat{\mathbf{x}}] + i\hat{\mathbf{p}} = [\hat{V}, \hat{\mathbf{x}}]$ (in atomic units) for the transitions that the absolute gauge error satisfies

$$\Delta_{L,V} = \frac{1}{\omega} \int r^3 R_{n_f,\ell_f} R_{n_i,\ell_i} \left(V_{\ell_f} - V_{\ell_i} \right) dr, \qquad (9)$$

with final- and initial-state radial wave functions R_{n_f,ℓ_f} and R_{n_i,ℓ_i} and model potentials V_ℓ (which we take from Ref. [29]). The integral vanishes for $\ell_< \geqslant 3$ because, in that case, the potentials do not depend on ℓ. Otherwise, the integral is nonzero and accumulates substantially only at short distances, where the potentials are strongly ℓ dependent and the wave functions are approximately shape invariant in n, with amplitudes scaling as $n^{-3/2}$. Since the $1/\omega$ prefactor scales as n^3, the n scalings cancel. Hence, $\Delta_{L,V}$ is approximately fixed within any given series. Numerical integration of Eq. (9) yields results that agree with the differences between the matrix elements to within typically three digits after the decimal point (in atomic units), in accordance with the numerical uncertainty of the matrix elements of five digits or better. For the strongest transitions, the values of $\Delta_{L,V}$ vary between $n = 15$ and $n = 100$ as follows: For $nD \leftrightarrow (n+1)P$, $\Delta_{L,V} = -0.327 \, ea_0$ to $-0.343 \, ea_0$, for $nS \leftrightarrow nP$, $\Delta_{L,V} = -0.0610 \, ea_0$ to $-0.0615 \, ea_0$, for $nS \leftrightarrow (n-1)P$,

$\Delta_{L,V} = -0.0565 \, ea_0$ to $-0.0575 \, ea_0$, and for $nD \leftrightarrow (n-1)F$, $\Delta_{L,V} = -0.0746 \, ea_0$ to $-0.0720 \, ea_0$. The integral in Eq. (9) reaches its asymptotic value to within 0.1% typically over a range of only $8a_0$. These findings prove that the VG matrix elements follow from the LG ones by subtracting an approximately n-independent and series-dependent value, given by Eq. (9). Furthermore, the agreement of the results from Eq. (9) with the data in Fig. 2 serves as a consistency check.

Along similar lines, in Fig. 2 it may seem at first unexpected that $\Delta_{L,V}$ is near-constant even across the Cooper-like minima of the EDTMs. Equation (9) shows that the near-constant, absolute gauge error is given by an integral that accumulates within less than $10a_0$. In contrast, the Cooper-like minima largely depend on the quantum-defect-dependent relative positions of Rydberg wave-function maxima and minima in the outer reaches of the atom. Therefore, gauge error and Cooper-like minima are quite unrelated, and the gauge error is not expected to exhibit any unusual behavior across the Cooper-like minima.

Equation (9) further shows that fine-structure energy shifts have no significant effect on $\Delta_{L,V}$, because the radial wave functions $R_{n,\ell,j}$ have virtually no dependence on j at radial positions of less than $10a_0$.

As a practical matter, we note that the $1/\omega$ dependence of M_V [see Eq. (5)] causes numerical inaccuracy for near-degenerate transitions, for which the integral expression in Eq. (5) can drop to near or even below its numerical error. As a result, for sufficiently degenerate transitions the expression in Eq. (5) becomes numerically unstable. Since the LG form [Eq. (6)] has no such numerical problem, the frequency-denominator issue is of no practical concern. For $\ell_< \leqslant 2$, where the VG form *must* be used, there are no near-degenerate transitions, so the issue does not arise, while for $\ell_< \geqslant 3$, where near-degenerate transitions occur when $\Delta n = 0$, the LG form may used.

The limiting case of resonant transitions with $\omega \to 0$, which occurs in transitions with $\Delta n = 0$ and large values of ℓ, requires additional caution because of the rise of Bloch-Siegert shifts caused by the counter-rotating terms [51] and other complications. The counter-rotating terms have been dropped early on in our analysis when making the rotating-wave approximation.

Following the discussion, we are using the method summarized in Fig. 1 to pick EDTMs for any electric-dipole transition of interest. First, we compute databases $M_V(n_i, l_i, \Delta n, \Delta_\ell)$ and $M_L(n_i, l_i, \Delta n, \Delta_\ell)$. After entering the transition labels $(n_i, l_i, \Delta n, \Delta\ell)$, the following simple rules are applied:

  i. If $\ell_< \leqslant 2$, pick $M_V(n_i, l_i, \Delta n, \Delta_\ell)$.

  ii. If $\ell_< \geqslant 3$ and $|\Delta n| \geqslant 1$, use the average of $M_V(n_i, l_i, \Delta n, \Delta_\ell)$ and $M_L(n_i, l_i, \Delta n, \Delta_\ell)$.

  iii. If $\ell_< \geqslant 3$ and $|\Delta n| = 0$, pick $M_L(n_i, l_i, \Delta n = 0, \Delta_\ell)$.

Next we discuss the consequences of our findings. For the strongest transitions within the $\ell_< \leqslant 2$ series displayed in Fig. 2, the choice of the gauge form does not play an overwhelming role, as $\delta_{L,V}$—the relative EDTM error incurred by adopting the LG instead of the VG form—barely exceeds 10^{-3} even in the worst cases. It will be fairly challenging to spectroscopically probe Rabi-frequency discrepancies at that

level of precision (and to even calibrate rf electric fields with sufficient accuracy to enable such measurements). At the same time, note that high precision is critical sometimes , such as in implementing quantum gates with microwave pulses [52–55] and in metrology applications. In the latter, the atom-field coupling amplitude has to be known better than to three or four significant digits. This is the case, for instance, in applications of Rydberg atoms in defining voltage standards [56,57]. In those specialized applications, the gauge error discussed in the present work will become relevant.

We also wish to point out that the gauge errors follow from the model potentials entered into the computation. As such, experimental data on the gauge effects would provide information on the accuracy of the potentials and, therefore, provide a test for the modeling of atomic many-electron systems. The relative gauge errors near the Cooper-like minima in Fig. 2 are quite significant. Measurements of EDTMs for several n_i near the Cooper-like minima may offer an experimental opportunity to explore these minima and gauge effects in Rydberg EDTMs. The same holds for photoionization cross sections, which show Cooper minima the wavelengths of which depend on the gauge form used in the bound-free EDTM calculation [27,28].

V. CONCLUSION

We have presented results for EDTMs calculated in three different gauge forms: velocity, length, and acceleration. Based on the analysis of the observed differences between these forms, we outlined a method for choosing the most appropriate gauge form, depending on the quantum numbers of the transition. We have discussed aspects of the underlying physics. We provide a concise equation for $\Delta_{L,V}$—Eq. (9)—that proves that the absolute gauge er-

ror $\Delta_{L,V}$ should not strongly depend on n within any given series.

In the computations we have used model potentials for Rb from Ref. [29]. Analogous computations could be performed for cesium or other alkali atoms for which there is a set of model potentials.

We point out a difference between resonant and off-resonant interaction. The quadratic DC and AC Stark effects occur off-resonantly, including the case $\omega = 0$ for the DC Stark effect. Off-resonant Stark shifts are best evaluated in the length gauge [34], in which the EDTMs in length-gauge form are exact. For resonant interactions, which we have considered here, the EDTMs in velocity-gauge form are exact.

The observed differences between the gauge forms have negligible or only minor consequences in applications of Rydberg atoms for microwave field sensing [10–13], where strong transitions are used. For these, the relative gauge error, $\delta_{L,V}$, remains below $\approx 10^{-3}$. The small differences between these EDTMs are likely to become relevant in precision measurements of resonant AC versus off-resonant AC or DC electric fields, including applications of Rydberg atoms in defining voltage standards [56,57].

Several of the weak transition series have relative gauge errors of 1% and up. These large relative gauge errors may be observable in experimental line strength measurements on weak transition series.

[1] T. F. Gallagher, *Rydberg Atoms* (Cambridge University Press, 2005), Vol. 3.

[2] J. Hare, A. Nussenzweig, C. Gabbanini, M. Weidemuller, P. Goy, M. Gross, and S. Haroche, Toward a Rydberg constant measurement on circular atoms, IEEE Trans. Instrum. Meas. **42**, 331 (1993).

[3] U. D. Jentschura, P. J. Mohr, and J. N. Tan, Fundamental constants and tests of theory in Rydberg states of one-electron ions, J. Phys. B: At., Mol. Opt. Phys. **43**, 074002 (2010).

[4] A. Ramos, K. Moore, and G. Raithel, Measuring the Rydberg constant using circular Rydberg atoms in an intensity-modulated optical lattice, Phys. Rev. A **96**, 032513 (2017).

[5] S. J. Berl, C. A. Sackett, T. F. Gallagher, and J. Nunkaew, Core polarizability of rubidium using spectroscopy of the ng to nh, ni Rydberg transitions, Phys. Rev. A **102**, 062818 (2020).

[6] J. P. Shaffer, S. T. Rittenhouse, and H. R. Sadeghpour, Ultracold Rydberg molecules, Nat. Commun. **9**, 1965 (2018).

[7] C. Fey, F. Hummel, and P. Schmelcher, Ultralong-range Rydberg molecules, Mol. Phys. **118**, e1679401 (2020).

[8] N. Thaicharoen, K. R. Moore, D. A. Anderson, R. C. Powel, E. Peterson, and G. Raithel, Electromagnetically induced transparency, absorption, and microwave-field sensing in a Rb vapor cell with a three-color all-infrared laser system, Phys. Rev. A **100**, 063427 (2019).

[9] R. Cardman and G. Raithel, Circularizing Rydberg atoms with time-dependent optical traps, Phys. Rev. A **101**, 013434 (2020).

[10] J. A. Sedlacek, A. Schwettmann, H. Kübler, R. Löw, T. Pfau, and J. P. Shaffer, Microwave electrometry with Rydberg atoms in a vapour cell using bright atomic resonances, Nat. Phys. **8**, 819 (2012).

[11] C. L. Holloway, J. A. Gordon, S. Jefferts, A. Schwarzkopf, D. A. Anderson, S. A. Miller, N. Thaicharoen, and G. Raithel, Broadband Rydberg atom-based electric-field probe for SI-traceable, self-calibrated measurements, IEEE Trans. Antennas Propag. **62**, 6169 (2014).

[12] D. A. Anderson, R. E. Sapiro, and G. Raithel, A self-calibrated si-traceable Rydberg atom-based radio frequency electric field probe and measurement instrument, IEEE Trans. Antennas Propag. **69**, 5931 (2021).

[13] D. A. Anderson, R. E. Sapiro, and G. Raithel, Rydberg atoms for radio-frequency communications and sensing: Atomic receivers for pulsed rf field and phase detection, IEEE Aerosp. Electron. Syst. Mag. **35**, 48 (2020).

[14] D. E. Chang, V. Vuletić, and M. D. Lukin, Quantum nonlinear optics—photon by photon, Nat. Photonics **8**, 685 (2014).

[15] Q.-Y. Liang, A. V. Venkatramani, S. H. Cantu, T. L. Nicholson, M. J. Gullans, A. V. Gorshkov, J. D. Thompson, C. Chin, M. D. Lukin, and V. Vuletić, Observation of three-photon bound states in a quantum nonlinear medium, Science **359**, 783 (2018).

[16] S. H. Cantu, A. V. Venkatramani, W. Xu, L. Zhou, B. Jelenković, M. D. Lukin, and V. Vuletić, Repulsive photons in a quantum nonlinear medium, Nat. Phys. **16**, 921 (2020).

[17] M. Saffman, Quantum computing with atomic qubits and Rydberg interactions: Progress and challenges, J. Phys. B: At., Mol. Opt. Phys. **49**, 202001 (2016).

[18] A. Browaeys and T. Lahaye, Many-body physics with individually controlled Rydberg atoms, Nat. Phys. **16**, 132 (2020).

[19] M. Morgado and S. Whitlock, Quantum simulation and computing with Rydberg-interacting qubits, AVS Quantum Sci. **3**, 023501 (2021).

[20] C. S. Adams, J. D. Pritchard, and J. P. Shaffer, Rydberg atom quantum technologies, J. Phys. B: At., Mol. Opt. Phys. **53**, 012002 (2019).

[21] M. S. Safronova, C. J. Williams, and C. W. Clark, Relativistic many-body calculations of electric-dipole matrix elements, lifetimes, and polarizabilities in rubidium, Phys. Rev. A **69**, 022509 (2004).

[22] N. Šibalić, J. D. Pritchard, C. S. Adams, and K. J. Weatherill, Arc: An open-source library for calculating properties of alkali Rydberg atoms, Comput. Phys. Commun. **220**, 319 (2017).

[23] M. S. Safronova and U. I. Safronova, Critically evaluated theoretical energies, lifetimes, hyperfine constants, and multipole polarizabilities in ^{87}Rb, Phys. Rev. A **83**, 052508 (2011).

[24] Y.-J. Chen, L. F. Gonçalves, and G. Raithel, Measurement of Rb $5P_{3/2}$ scalar and tensor polarizabilities in a 1064-nm light field, Phys. Rev. A **92**, 060501(R) (2015).

[25] T. P. Dinneen, C. D. Wallace, K.-Y. N. Tan, and P. L. Gould, Use of trapped atoms to measure absolute photoionization cross sections, Opt. Lett. **17**, 1706 (1992).

[26] F. Markert, P. Würtz, A. Koglbauer, T. Gericke, A. Vogler, and H. Ott, ac-Stark shift and photoionization of Rydberg atoms in an optical dipole trap, New J. Phys. **12**, 113003 (2010).

[27] M. A. Viray, E. Paradis, and G. Raithel, Photoionization of nS and nD Rydberg atoms of Rb and Cs from the near-infrared to the ultraviolet spectral region, New J. Phys. **23**, 063022 (2021).

[28] R. Cardman, J. L. MacLennan, S. E. Anderson, Y.-J. Chen, and G. Raithel, Photoionization of Rydberg atoms in optical lattices, New J. Phys. **23**, 063074 (2021).

[29] M. Marinescu, H. R. Sadeghpour, and A. Dalgarno, Dispersion coefficients for alkali-metal dimers, Phys. Rev. A **49**, 982 (1994).

[30] H. A. Bethe and E. E. Salpeter, *Quantum Mechanics of One- and Two-Electron Atoms* (Springer-Verlag, Berlin, 2014).

[31] H. Friedrich, *Theoretical Atomic Physics* (Springer International, Cham, 2017).

[32] A. Papoulia, J. Ekman, G. Gaigalas, M. Godefroid, S. Gustafsson, H. Hartman, W. Li, L. Radžiūtė, P. Rynkun, S. Schiffmann, K. Wang, and P. Jönsson, Coulomb (velocity) gauge recommended in multiconfiguration calculations of transition data involving Rydberg series, Atoms **7**, 106 (2019).

[33] J. J. Sakurai and J. Napolitano, *Modern Quantum Mechanics*, 2nd ed. (Cambridge University Press, Cambridge, 2017).

[34] T. Topcu and A. Derevianko, Dynamic polarizability of Rydberg atoms: Applicability of the near-free-electron approximation, gauge invariance, and the Dirac sea, Phys. Rev. A **88**, 042510 (2013).

[35] I. P. Grant, Gauge invariance and relativistic radiative transitions, J. Phys. B: At. Mol. Phys. **7**, 1458 (1974).

[36] C. Froese Fischer, Evaluating the accuracy of theoretical transition data, Phys. Scr. **T134**, 014019 (2009).

[37] C. Leone, S. Bivona, R. Burlon, F. Morales, and G. Ferrante, Gauge aspects in multichannel multiphoton ionization, Phys. Rev. A **40**, 1828 (1989).

[38] E. Cormier and P. Lambropoulos, Optimal gauge and gauge invariance in non-perturbative time-dependent calculation of above-threshold ionization, J. Phys. B: At., Mol. Opt. Phys. **29**, 1667 (1996).

[39] D. Bauer, D. B. Milošević, and W. Becker, Strong-field approximation for intense-laser–atom processes: The choice of gauge, Phys. Rev. A **72**, 023415 (2005).

[40] Y. J. Chen and B. Hu, Strong-field approximation for diatomic molecules: Comparison between the length gauge and the velocity gauge, Phys. Rev. A **80**, 033408 (2009).

[41] Y.-C. Han and L. B. Madsen, Comparison between length and velocity gauges in quantum simulations of high-order harmonic generation, Phys. Rev. A **81**, 063430 (2010).

[42] A. D. Bandrauk, F. Fillion-Gourdeau, and E. Lorin, Atoms and molecules in intense laser fields: Gauge invariance of theory and models, J. Phys. B: At., Mol. Opt. Phys. **46**, 153001 (2013).

[43] K. S. Virk and J. E. Sipe, Semiconductor optics in length gauge: A general numerical approach, Phys. Rev. B **76**, 035213 (2007).

[44] D. J. Passos, G. B. Ventura, J. M. Viana Parente Lopes, J. M. B. Lopes dos Santos, and N. M. R. Peres, Nonlinear optical responses of crystalline systems: Results from a velocity gauge analysis, Phys. Rev. B **97**, 235446 (2018).

[45] A. Pehlivan Rhodin, H. Hartman, H. Nilsson, and P. Jönsson, Experimental and theoretical oscillator strengths of Mg I for accurate abundance analysis, Astron. Astrophys. **598**, A102 (2017).

[46] S. K. Dutta, J. R. Guest, D. Feldbaum, A. Walz-Flannigan, and G. Raithel, Ponderomotive Optical Lattice for Rydberg Atoms, Phys. Rev. Lett. **85**, 5551 (2000).

[47] S. E. Anderson, K. C. Younge, and G. Raithel, Trapping Rydberg Atoms in an Optical Lattice, Phys. Rev. Lett. **107**, 263001 (2011).

[48] A. Reinhard, T. C. Liebisch, B. Knuffman, and G. Raithel, Level shifts of rubidium Rydberg states due to binary interactions, Phys. Rev. A **75**, 032712 (2007).

[49] See Supplemental Material at http://link.aps.org/supplemental/10.1103/PhysRevA.105.012825 for the computed transition matrix elements in length and velocity gauges used in Fig. 2 as well as the energy differences between the states involved in the corresponding transitions.

[50] J. W. Cooper, Photoionization from outer atomic subshells. A model study, Phys. Rev. **128**, 681 (1962).

[51] P. Berman and V. Malinovsky, *Principles of Laser Spectroscopy and Quantum Optics* (Princeton University Press, Princeton, 2011).

[52] I. I. Beterov, M. Saffman, E. A. Yakshina, V. P. Zhukov, D. B. Tretyakov, V. M. Entin, I. I. Ryabtsev, C. W. Mansell, C. MacCormick, S. Bergamini, and M. P. Fedoruk, Quan-

tum gates in mesoscopic atomic ensembles based on adiabatic passage and Rydberg blockade, Phys. Rev. A **88**, 010303(R) (2013).

[53] J. D. Pritchard, J. A. Isaacs, M. A. Beck, R. McDermott, and M. Saffman, Hybrid atom-photon quantum gate in a superconducting microwave resonator, Phys. Rev. A **89**, 010301(R) (2014).

[54] C. Hermann-Avigliano, R. C. Teixeira, T. L. Nguyen, T. Cantat-Moltrecht, G. Nogues, I. Dotsenko, S. Gleyzes, J. M. Raimond, S. Haroche, and M. Brune, Long coherence times for Rydberg qubits on a superconducting atom chip, Phys. Rev. A **90**, 040502(R) (2014).

[55] D. Petrosyan, F. Motzoi, M. Saffman, and K. Mølmer, High-fidelity Rydberg quantum gate via a two-atom dark state, Phys. Rev. A **96**, 042306 (2017).

[56] R. Sapiro, G. Raithel, and D. Anderson, Atom-based optical RF-power/voltage transducer and sensor, in *APS Division of Atomic, Molecular and Optical Physics Meeting Abstracts* (APS Meeting Abstracts, 2019), Vol. 2019, p. L01.031.

[57] C. L. Holloway, N. Prajapati, J. Kitching, J. A. Sherman, C. Teale, A. Rufenacht, A. B. Artusio-Glimpse, M. T. Simons, A. K. Robinson, and E. B. Norrgard, Electromagnetically induced transparency based Rydberg-atom sensor for quantum-based voltage measurements, arXiv:2110.02335.